Z. Angew. Math. Phys. 64 (2013), 1759–1777

0044-2275/13/061759-19
published online August 20, 2013
DOI 10.1007/s00033-013-0355-8

Zeitschrift für angewandte Mathematik und Physik ZAMP

Motion of a distant solid particle in a shear flow along a porous slab

S. Khabthani, A. Sellier and F. Feuillebois

Abstract. The motion of a solid and no-slipping particle immersed in a shear flow along a sufficiently porous slab is investigated. The fluid flow outside and inside of the slab is governed by the Stokes and Darcy equations, respectively, and the so-called Beavers and Joseph slip boundary conditions are enforced on the slab surface. The problem is solved for a distant particle with length scale a in terms of the small parameter a/d where d designates the large particle–slab separation. This is achieved by asymptotically inverting a relevant boundary-integral equation on the particle surface, which has been recently proposed for any particle location (distant or close particle) in Khabthani et al. (J Fluid Mech 713:271–306, 2012). It is found that at order $O(a/d)$ the slab behaves for any particle shape as a solid plane no-slip wall while the slab properties (thickness, permeability, associated slip length) solely enter at $O((a/d)^2)$. Moreover, for a spherical particle, the numerical results published in Khabthani et al. (J Fluid Mech 713:271–306, 2012) perfectly agree with the present asymptotic analysis.

Mathematics Subject Classification (2010). 34E05 · 45B05 · 76D07 · 76S05.

Keywords. Stokes flow · Darcy flow · Beavers and Joseph slip boundary condition · Asymptotic analysis.

1. Introduction

Many basic applications require to predict the non-trivial rheology (effective viscosity, ...) of flowing and bounded suspensions made of solid (but not-necessarily spherical) particles suspended in a Newtonian fluid. One may for instance think about the open flow of a suspension above a plane solid wall (case of only one boundary) or between two parallel plane solid walls (case of two different boundaries). In general, such a task is tremendously involved and requires extensive direct and three-dimensional numerical simulations of the Navier–Stokes equations.

Fortunately, for sufficiently dilute suspensions, it is possible to neglect particle–particle interactions. In addition, whenever the separation between two boundaries is much larger than the particles' typical length scale a, one ends up with the much more tractable problem of one particle interacting with a motionless and either plane or curved boundary Σ. As depicted in Fig. 1, we confine here our attention to a plane surface Σ, namely the $x_3 = 0$ plane upper boundary of a given and motionless semi-infinite or bounded medium. We shall also use Cartesian coordinates (O, x_1, x_2, x_3) with origin O located on the surface Σ.

Above the boundary Σ (for $x_3 > 0$), the flow about the solid particle with given shape and location has a pressure field Q and a velocity field $\mathbf{v}$ with Cartesian components $v_i = \mathbf{v} \cdot \mathbf{e}_i$. Conditions on the surface Σ deeply depend upon the type of boundary (permeable or impermeable surface, rough or smooth surface). When Σ is impermeable and slipping (as in Fig. 1a), one widely adopts the [2] slip conditions

$$v_1 = \lambda \frac{\partial v_1}{\partial x_3}, \quad v_2 = \lambda \frac{\partial v_2}{\partial x_3} \quad \text{and} \quad v_3 = 0 \text{ at } \Sigma(x_3 = 0) \tag{1}$$

where $\lambda \geq 0$ is the (effective) boundary slip length that may be seen as the distance at which the velocity vanishes when extrapolated inside the solid medium. The conditions (1) are well experimentally

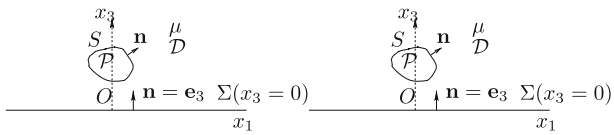

FIG. 1. A solid particle $\mathcal{P}$ immersed in a Newtonian fluid above a motionless and impermeable solid (**a**) or a porous (**b**) medium with upper-plane boundary Σ

supported [3,4] and valid, for instance, for hydrophobic boundaries. Note that for $\lambda = 0$ one retrieves the usual no-slip velocity condition $\mathbf{v} = \mathbf{0}$ at a plane impermeable wall.

When Σ turns out to be *permeable* (considering for instance a membrane), the relations (1) are not valid any more. Relevant boundary conditions at a permeable surface Σ depend upon the nature of the medium located in the $x_3 < 0$ domain. For a porous medium, the fluid also flows there with a pressure Q'' and a velocity $\mathbf{v}''$ with Cartesian components $v_i'' = \mathbf{v}'' \cdot \mathbf{e}_i$. Adopting for the porous medium the Darcy model, the equations to be applied are (*in the absence of gravity*) $\boldsymbol{\nabla} \cdot \mathbf{v}'' = 0$ and $\mathbf{v}'' = -K\boldsymbol{\nabla} Q''/\mu$ with $K > 0$ the so-called porous medium uniform permeability and μ the uniform fluid viscosity. One should note that for Darcy model, the length $\sqrt{K}$ is order of the typical pore size in the porous medium. Under these assumptions, one employs the following [5,6] boundary conditions

$$\frac{\partial v_1}{\partial x_3} = \frac{\sigma}{\sqrt{K}}(v_1 - v_1''), \frac{\partial v_2}{\partial x_3} = \frac{\sigma}{\sqrt{K}}(v_2 - v_2''), \quad v_3 = v_3'', \, Q = Q'' \quad \text{at} \quad \Sigma(x_3 = 0) \tag{2}$$

where the associated slip length $\sqrt{K}/\sigma$ is related to both the permeability $K > 0$ and another dimensionless coefficient $\sigma > 0$. Clearly, (2) encompasses (1) since one immediately recovers (1) by selecting $\sigma = \sqrt{K}/\lambda$ and letting $\sqrt{K}$ tend to zero so that $\mathbf{v}''$ vanishes. Related analytical works concern a sphere near a porous plane wall, but with the no-slip boundary condition along the wall: [7] solved the case of a sphere moving normally to a very thin porous membrane, and [8] considered the departure of a sphere from contact with a membrane; [9] solved the problem of a sphere moving towards a permeable half-space.

As for the use of Beavers and Joseph boundary conditions (2), the challenging case of a porous slab with uniform and finite thickness $e > 0$ (i.e. having for boundaries the $x_3 = 0$ and $x_3 = -e$ planes) has been recently handled in [1]. In that case, there is also a Stokes flow in the semi-infinite $x_3 < -e$ domain, and Beavers and Joseph boundary conditions analogous to (2) are required on the $x_3 = -e$ lower plane boundary. For the Darcy model to still hold in the slab ($-e < x_3 < 0$), it is moreover assumed that the slab thickness e is at least as large as the typical pore size $\sqrt{K}$. Under these assumptions, [1] considers the motion of a solid particle either experiencing a prescribed rigid-body motion or being freely suspended in a linear or quadratic ambient shear flow tangent to the slab. The particle–slab interactions for spherical and ellipsoidal particles are calculated by implementing a new "indirect boundary-integral" formulation. For a slab–particle separation of order d and a particle with typical length a, the particle–slab interactions were found to be strong for a close particle (d order a or less) and to quickly decay for a distant particle (as d/a becomes large).

The procedure advocated in [1] holds for arbitrarily shaped particles. It numerically inverts on the particle surface, employing curved 6-node triangular boundary elements, a Fredholm boundary-integral equation of the first kind with weakly singular and complicated kernel, the accuracy of which is good but is not adapted for adequately calculating the weak particle–slab interactions prevailing for a distant particle (i.e. for $g \gg a$). But, it is worth for applications to evaluate, at a reasonable cost, these weak particle–slab interactions in terms of the small parameter a/d and also to predict the sensitivity of those interactions to the dimensionless parameters $\sigma, a/e$ and $\sqrt{K}/e$. This challenging task has been done, using the bipolar coordinates method, for a distant sphere immersed in a linear [10] or quadratic [11] ambient shear flow tangent to a slipping and impermeable plane wall where the Navier slip conditions (1) are imposed (this is the case $1/e \to 0, \sigma = \sqrt{K}/\lambda$ and $\sqrt{K} \to 0$). In contrast, such asymptotic analysis

has not yet been achieved for the more challenging case of a porous slab with thickness e and subject to the Beaver and Joseph slip conditions (2) on its lower- and upper-plane boundaries. This work therefore addresses this key issue.

The paper is organized as follows. Governing equations and the indirect boundary formulation advocated in [1] for arbitrarily shaped and located (i.e. distant or not) particles are recalled in §2. The resulting asymptotic analysis for a distant and arbitrarily shaped particle is developed in §3. The case of a distant sphere is analytically worked out in §4 with comparisons against previous works [11–13] for a semi-infinite impermeable slipping wall subject to (1). In addition, the numerical results obtained in [1] for a solid sphere and a porous slab with thickness e and boundary conditions (2) are found to be in very good agreement with the asymptotic expansions presented in this paper.

2. Governing problem and boundary-integral formulation

This section presents the governing equations and the indirect boundary-integral formulation advocated in [1].

2.1. Addressed problems

As illustrated in Fig. 2, we consider a solid particle $\mathcal{P}$ with centre of mass O' and smooth surface S immersed in a Newtonian fluid above a motionless porous slab $\mathcal{S}$ with upper and lower parallel plane boundaries Σ_u and Σ_l, thickness $e > 0$ and permeability $K > 0$.

We employ Cartesian coordinates (O, x_1, x_2, x_3) with origin O located on the upper boundary Σ_u and such that $\mathbf{OO'} = d\mathbf{e}_3$ with $d > 0$. In addition, Σ_u and Σ_l are the $x_3 = 0$ and $x_3 = -e$ planes, respectively. The Newtonian fluid, with uniform density ρ_f and viscosity μ, and the particle are submitted to a uniform gravity field $\mathbf{g}$ and/or a prescribed ambient flow (such as the one depicted above the porous slab in Fig. 2) with, above the slab, a velocity $\mathbf{v}_\infty$ tangent to the slab and pressure p_∞. The particle rigid-body motion is described by its translational velocity $\mathbf{U}$ (the velocity of the centre of mass O') and angular velocity

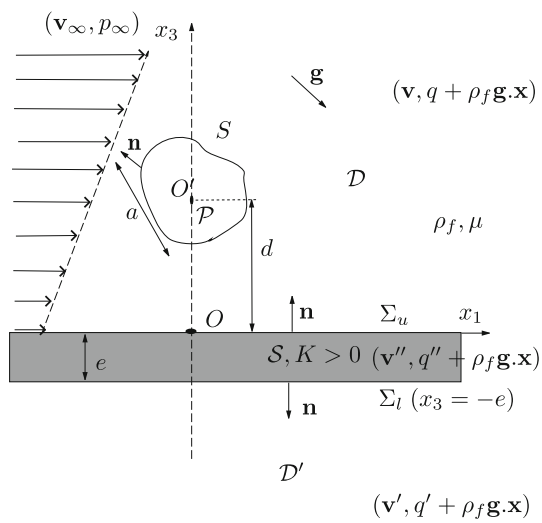

FIG. 2. A solid particle $\mathcal{P}$ with length scale a and centre of mass O' immersed in a viscous fluid above a porous slab $\mathcal{S}$ with thickness e and permeability $K > 0$, in a prescribed ambient shear (here linear) flow $(\mathbf{v}_\infty, p_\infty)$ and/or a uniform gravity field $\mathbf{g}$

$\boldsymbol{\Omega}$. The fluid flows in the porous slab with velocity $\mathbf{v}''$ and pressure $q'' + \rho_f \mathbf{g}\cdot\mathbf{x}$; in the domain $\mathcal{D}$ above the slab with velocity $\mathbf{v}$ and pressure $q + \rho_f \mathbf{g}\cdot\mathbf{x}$; and in the domain $\mathcal{D}'$ below the slab with velocity $\mathbf{v}'$ and pressure $q' + \rho_f \mathbf{g}\cdot\mathbf{x}$. Finally, the particle and the velocity field $\mathbf{v}$ above it have typical length scale a and magnitude V, respectively.

Assuming that $\mathrm{Re} = \rho_f V a/\mu \ll 1$, one can neglect all inertial effects and both flows $(\mathbf{v}, q)$ and $(\mathbf{v}', q')$ are steady Stokes flows. Using in the porous slab $\mathcal{S}$ the Darcy model,[1] the governing equations are

$$\mu\nabla^2\mathbf{v} = \boldsymbol{\nabla} q \quad \text{and} \quad \boldsymbol{\nabla}\cdot\mathbf{v} = 0 \ \text{ in } \mathcal{D}, \tag{3}$$

$$\mu\nabla^2\mathbf{v}' = \boldsymbol{\nabla} q' \quad \text{and} \quad \boldsymbol{\nabla}\cdot\mathbf{v}' = 0 \ \text{ in } \mathcal{D}', \tag{4}$$

$$\mathbf{v}'' = -K\boldsymbol{\nabla} q''/\mu \quad \text{and} \quad \boldsymbol{\nabla}\cdot\mathbf{v}'' = 0 \ \text{ in } \mathcal{S}. \tag{5}$$

Equations (3)–(5) are supplemented with the usual no-slip velocity condition on the particle surface and the Beavers and Joseph boundary conditions (recall (2)) on the porous slab boundaries

$$\mathbf{v} = \mathbf{U} + \boldsymbol{\Omega}\wedge\mathbf{O}'\mathbf{M} \quad \text{on } S, \tag{6}$$

$$\frac{\partial v_j}{\partial x_3} = \frac{\sigma}{\sqrt{K}}(v_1 - v_j'') \text{ for } j = 1,2;\ v_3 = v_3'',\ q = q'' \text{ at } \Sigma_u(x_3 = 0), \tag{7}$$

$$\frac{\partial v_j'}{\partial x_3} = -\frac{\sigma}{\sqrt{K}}(v_j' - v_j'') \text{ for } j = 1,2;\ v_3' = v_3'',\ q' = q'' \text{ at } \Sigma_l(x_3 = -e). \tag{8}$$

For convenience, consider the condensed notation $(\mathbf{w}, P)$ to designate a flow with velocity $\mathbf{w}$ and pressure P in the fluid domain above the porous slab. In a similar fashion, $(\mathbf{w}', P')$ and $(\mathbf{w}'', P'')$ are flows below and in the porous slab, respectively. For this work, the ambient flows are the following unidirectional flows $(\mathbf{v}_\infty, p_\infty)$, $(\mathbf{v}'_\infty, p'_\infty)$, and $(\mathbf{v}''_\infty, p''_\infty)$

$$\mathbf{v}_\infty = \{\gamma_1[x_3 + \sqrt{K}/\sigma] + \gamma_2[x_3^2 - 2K]\}\mathbf{e}_1 \quad \text{and} \quad p_\infty = 2\mu\gamma_2 x_1 \quad \text{for} \quad x_3 > 0, \tag{9}$$

$$\mathbf{v}'_\infty = \{\gamma_1'[x_3 + e - \sqrt{K}/\sigma] + \gamma_2[(x_3 + e)^2 - 2K]\}\mathbf{e}_1 \quad \text{and} \quad p'_\infty = 2\mu\gamma_2 x_1 \quad \text{for} \quad x_3 < -e, \tag{10}$$

$$\mathbf{v}''_\infty = -2\gamma_2 K\mathbf{e}_1 \quad \text{and} \quad p''_\infty = 2\mu\gamma_2 x_1 \quad \text{for} \quad -e < x_3 < 0. \tag{11}$$

As the reader may easily check, the selected flows $(\mathbf{v}_\infty, p_\infty)$, $(\mathbf{v}'_\infty, p'_\infty)$ and $(\mathbf{v}''_\infty, p''_\infty)$ satisfy (3)–(5) and (7)–(8) whatever the parameters γ_1, γ_1' and γ_2. Note also that $\mathbf{v}_\infty$ is the superposition of pure *linear* ($\gamma_2 = 0$) and *quadratic* ($\gamma_1 = 0$) shear flows parallel with the porous slab while γ_1' is not related to (γ_1, γ_2).

The particle affects each of the previous ambient flow through the no-slip requirement (6) and the coupling slip conditions (7)–(8). More precisely, the disturbed flow is $(\mathbf{v}_\infty + \mathbf{u}, p_\infty + p + \rho_f \mathbf{g}\cdot\mathbf{x})$ above the porous slab with $(\mathbf{u}, p)$ the flow disturbance. In a similar fashion, the flow below and in the slab is $(\mathbf{v}'_\infty + \mathbf{u}', p'_\infty + p' + \rho_f \mathbf{g}\cdot\mathbf{x})$ and $(\mathbf{v}''_\infty + \mathbf{u}'', p''_\infty + p'' + \rho_f \mathbf{g}\cdot\mathbf{x})$, respectively. By superposition, the flows $(\mathbf{u}, p)$, $(\mathbf{u}', p')$ and $(\mathbf{u}'', p'')$ obey the Eqs. (3)–(5), (7)–(8) and the far-field and boundary conditions

$$(\mathbf{u}, p) \to (\mathbf{0}, 0),\ (\mathbf{u}', p') \to (\mathbf{0}, 0),\ (\mathbf{u}'', p'') \to (\mathbf{0}, 0), \ \text{ as } |\mathbf{x}| \to \infty, \tag{12}$$

$$\mathbf{u} = \mathbf{u}_d = -\mathbf{v}_\infty + \mathbf{U} + \boldsymbol{\Omega}\wedge\mathbf{O}'\mathbf{M} \ \text{ on } S. \tag{13}$$

For further use, let us denote by $\boldsymbol{\sigma}$ the stress tensor of the perturbation flow $(\mathbf{u}, p)$ and by $\mathcal{V}$ the particle volume. Since $(\mathbf{v}_\infty, p_\infty)$ is a Stokes flow, it exerts zero net force and zero net torque on the particle surface S. Accordingly, the particle experiences hydrodynamic force $\mathbf{F}$ and torque $\boldsymbol{\Gamma}$ (about its *centre of mass* O') given by

[1] One should note that in the presence of a gravity field $\mathbf{g}$, the Darcy law for a flow in the porous slab with velocity $\mathbf{v}''$ and pressure Q'' then reads $\mathbf{v}'' = -K[\boldsymbol{\nabla} Q'' - \rho_f \mathbf{g}]/\mu$.

$$\mathbf{F} = \int_S \boldsymbol{\sigma}\cdot\mathbf{n}\mathrm{d}S - \rho_f\mathcal{V}\mathbf{g},\ \boldsymbol{\Gamma} = \int_S \mathbf{x}'\wedge\boldsymbol{\sigma}\cdot\mathbf{n}\mathrm{d}S \tag{14}$$

where $\mathbf{x}' = \mathbf{O}'\mathbf{M}$ and $\mathbf{n}$ designates (see Fig. 2) the unit normal on the particle surface pointing into the fluid domain.

At this stage, two different cases arise:

(i) The case of a solid particle experiencing, *in the absence of gravity*, a prescribed rigid-body migration $(\mathbf{U},\boldsymbol{\Omega})$ in a *quiescent* fluid ($\gamma_1 = \gamma_2 = \gamma_1' = 0$ and $\mathbf{g} = \mathbf{0}$). One then solves for the flow $(\mathbf{u}, p)$ by using (3)–(8), (12)–(13) and taking $\mathbf{v}_\infty = \mathbf{0}$ in (13). Results allow us to compute the net force and net torque $\mathbf{F}$ and $\boldsymbol{\Gamma}$, which here admit, by linearity, the following forms:

$$\mathbf{F} = -\mu[\mathbf{A}\cdot\mathbf{U} + \mathbf{B}\cdot\boldsymbol{\Omega}],\ \boldsymbol{\Gamma} = -\mu[\mathbf{C}\cdot\mathbf{U} + \mathbf{D}\cdot\boldsymbol{\Omega}] \tag{15}$$

where $\mathbf{A}, \mathbf{B}, \mathbf{C}$ and $\mathbf{D}$ are the so-called second-rank resistance tensors. Because of the Beavers and Joseph coupling conditions (7)–(8), the tensors $\mathbf{B}$ and $\mathbf{C}$ are not in general transposed (see [1]).

(ii) The case of a solid particle *held fixed* in the ambient flow $(\mathbf{v}_\infty, q_\infty)$ *in the absence of gravity.* Once the flow $(\mathbf{u}, p)$ is obtained, now by setting $\mathbf{U} = \boldsymbol{\Omega} = \mathbf{0}$ in (13), it is then possible to calculate the resulting force and torque on the particle using (14) for $\mathbf{g} = \mathbf{0}$. Those force and torque, further denoted by $\mathbf{F}_a$ and $\boldsymbol{\Gamma}_a$, depend upon the applied ambient velocity field $\mathbf{v}_\infty$.

By superposition, the treatment of the previous Cases (i)–(ii) immediately provides a linear system for the unknown rigid-body motion $(\mathbf{U},\boldsymbol{\Omega})$ of a particle freely suspended in prescribed ambient flow $\mathbf{v}_\infty$ and gravity field $\mathbf{g}$. Assuming a particle with uniform density ρ_s and requiring it to be force-free and torque-free, one indeed obtains

$$\mu[\mathbf{A}\cdot\mathbf{U} + \mathbf{B}\cdot\boldsymbol{\Omega}] = \mathbf{F}_a + (\rho_s - \rho_f)\mathcal{V}\mathbf{g},\ \mu[\mathbf{C}\cdot\mathbf{U} + \mathbf{D}\cdot\boldsymbol{\Omega}] = \boldsymbol{\Gamma}_a. \tag{16}$$

2.2. Associated Green tensor and indirect boundary-integral approach

A new indirect boundary formulation has been proposed in [1] to numerically solve the key previous Cases (i)–(ii). Here, we briefly introduce this approach while directing for further details the reader to [1].

In a first step, a relevant Green tensor induced by a point force with intensity $\mathbf{e}_k$ located at a source point $\mathbf{y}$ above the porous slab is obtained. This source induces above, in and below the porous slab three flows that have to satisfy the far-field behaviour (12) and the coupling Beavers and Joseph boundary conditions (7)–(8). At a point $\mathbf{x}$ located above the porous slab, the resulting flow velocity reads $\mathbf{G}(\mathbf{x},\mathbf{y})\cdot\mathbf{e}_k/[8\pi\mu]$ where the so-called second-rank Green tensor $\mathbf{G}$ has Cartesian component $G_{jk}(\mathbf{x},\mathbf{y})$. In the absence of porous slab (unbounded fluid), the Green tensor $\mathbf{G}^\infty(\mathbf{x},\mathbf{y})$, free from the conditions (7)–(8), is the weakly singular Oseen–Burgers tensor such that

$$G^\infty_{jk}(\mathbf{x},\mathbf{y}) = \frac{\delta_{jk}}{|\mathbf{x}-\mathbf{y}|} + \frac{[(\mathbf{x}-\mathbf{y})\cdot\mathbf{e}_j][(\mathbf{x}-\mathbf{y})\cdot\mathbf{e}_k]}{|\mathbf{x}-\mathbf{y}|^3} \tag{17}$$

with δ_{jk} the kronecker delta. The simple solution (17) is the so-called Stokeslet with intensity $\mathbf{e}_k$ located at point $\mathbf{y}$. When there is a porous slab and (7)–(8) hold, the solution is obtained as

$$G_{jk}(\mathbf{x},\mathbf{y}) = G^\infty_{jk}(\mathbf{x},\mathbf{y}) + R_{jk}(\mathbf{x},\mathbf{y}) \tag{18}$$

with regular Cartesian components $R_{jk}(\mathbf{x},\mathbf{y})$ given in [1]. Before displaying these components, we introduce the symmetric $\mathbf{y}_s$ of the pole $\mathbf{y}$ with respect to the plane Σ_u (see Fig. 3), the symbol $\mathcal{J}_{kl} = \delta_{k1}\delta_{1l} + \delta_{k2}\delta_{2l} - \delta_{k3}\delta_{3l}$, the vector $\mathbf{R}' = \mathbf{x} - \mathbf{y}_s$ and the quantities $R'_j = \mathbf{R}'\cdot\mathbf{e}_j, \rho = \sqrt{R_1'^2 + R_2'^2}$.

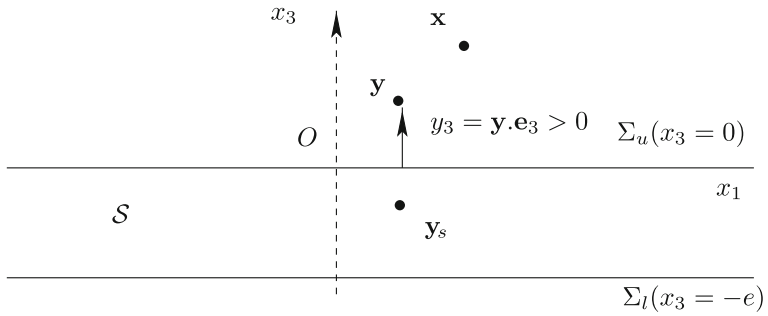

FIG. 3. A pole $\mathbf{y}$ and its symmetric $\mathbf{y}_s$ with respect to the plane $\Sigma_u(x_3 = 0)$ upper boundary of the porous slab $\mathcal{S}$

Note that $R'_3 = x_3 + y_3$. Hence, for a pole $\mathbf{y}$ and a so-called observation point $\mathbf{x}$ both located above the porous slab, one gets $R'_3 > 0$. The following transform is used in the solution:

$$\langle g\rangle(\rho, R'_3) = \int_0^\infty J_0(\rho\xi) e^{-R'_3\xi} g(\xi)\,\mathrm{d}\xi \tag{19}$$

where J_0 denotes the zeroth-order Bessel function. Under these notations, the results obtained in [1] read

$$\begin{aligned} R_{jk}(\mathbf{x},\mathbf{y}) = {} & -G^\infty_{jk}(\mathbf{x},\mathbf{y}_s) \\ & + \left[\delta_{3j} - x_3\frac{\partial}{\partial R'_j}\right]\left\{\mathcal{J}_{kl}\frac{\partial\langle f_1\rangle}{\partial R'_l} + \delta_{3k}\left(\frac{\partial\langle f_2\rangle}{\partial R'_3} + \langle f_3\rangle\right)\right\} \\ & + \left[2\sigma\sqrt{K}\frac{\partial}{\partial R'_3} - 1\right]\left\{\mathcal{J}_{kl}\frac{\partial^2\langle f_4\rangle}{\partial R'_j\partial R'_l} + \delta_{3k}\left(\frac{\partial^2\langle f_5\rangle}{\partial R'_3\partial R'_j} + \frac{\partial\langle f_6\rangle}{\partial R'_j}\right)\right\} \\ & + \left\{\delta_{3k}\delta_{jl}\sigma y_3 + 2\sqrt{K}(\delta_{3l}\mathcal{J}_{kj} - \delta_{3j}\mathcal{J}_{kl}) + \left[2K\sigma\delta_{3k}\delta_{3l} - y_3\sqrt{K}(\mathcal{J}_{kl} + \delta_{3k}\delta_{3l})\right]\frac{\partial}{\partial R'_j}\right\}\frac{\partial\langle f_7\rangle}{\partial R'_l} \end{aligned} \tag{20}$$

with functions $f_1, \ldots, f_7$ depending upon (e, K, σ, y_3) and given in Appendix A. Of course, there is a summation over repeated indices $l = 1, 2, 3$ in (20). As seen from (18) and (20), the Green tensor $\mathbf{G}$ is the superposition of a Stokeslet with intensity $\mathbf{e}_k$ located at the source $\mathbf{y}$, a Stokeslet image with intensity $-\mathbf{e}_k$ located at the symmetric point $\mathbf{y}_s$ and another regular tensor involving the functions $f_1, \ldots, f_7$.

The second step consists in employing for the velocity field $\mathbf{u}$ above the porous slab the single-layer integral representation

$$\mathbf{u}(\mathbf{x}) = -\frac{1}{8\pi\mu}\int_S \mathbf{G}(\mathbf{x},\mathbf{y})\cdot\mathbf{d}(\mathbf{y})\mathrm{d}S \quad \text{for } \mathbf{x} \text{ in } \mathcal{D} \tag{21}$$

with $\mathbf{d}$ an unknown surface density. In a similar fashion, the pressure p in the fluid domain $\mathcal{D}$ also receives, in terms of $\mathbf{d}$, another integral representation. Since it is useless in the present paper, such a representation is, however, not given here.

The flow $(\mathbf{u}, p)$ exerts on the particle surface S a stress $\mathbf{f} = \boldsymbol{\sigma}\cdot\mathbf{n}$. One should take notice that $\mathbf{d}$ is different from $\mathbf{f}$. Nevertheless, as shown in [1], it turns out that the force and torque (about O') given by (14) are related to the density $\mathbf{d}$ as follows:

$$\mathbf{F} = \int_S \mathbf{d}\mathrm{d}S - \rho_f\mathcal{V}\mathbf{g},\ \boldsymbol{\Gamma} = \int_S \mathbf{x}'\wedge\mathbf{d}\mathrm{d}S. \tag{22}$$

Accordingly, calculating the surface density $\mathbf{d}$ is sufficient to solve Cases (i)–(ii) introduced in §2.1. This is achieved by enforcing the boundary condition (13) at the particle surface, therefore arriving at the following Fredholm boundary-integral equation of the first kind

$$\mathbf{u}_d = -\frac{1}{8\pi\mu}\int_S \mathbf{G}(\mathbf{x},\mathbf{y})\cdot\mathbf{d}(\mathbf{y})\mathrm{d}S \text{ for } \mathbf{x} \text{ on } S,\ \mathbf{u}_d = -\mathbf{v}_\infty + \mathbf{U} + \boldsymbol{\Omega}\wedge\mathbf{x}'. \tag{23}$$

In summary, the task reduces to the treatment of the boundary-integral equation (23) with Green tensor $\mathbf{G}$ given by (18) and (20). As noticed earlier, the tensor $\mathbf{R}$ arising in the decomposition (18) is regular in the entire domain above the porous slab. Consequently, the following identity holds:

$$\int_S \mathbf{G}(\mathbf{x},\mathbf{y})\cdot\mathbf{n}(\mathbf{x})\mathrm{d}S = \mathbf{0} \quad \text{for} \quad \mathbf{x}\cdot\mathbf{e}_3 > 0. \tag{24}$$

Moreover, the definition of the velocity $\mathbf{u}_d$ ensures that

$$\int_S [\mathbf{u}_d\cdot\mathbf{n}](\mathbf{y})\mathrm{d}S = 0. \tag{25}$$

Accordingly, under the so-called compatibility relation (25), the boundary-integral equation (23) admits a solution $\mathbf{d}$. It has been numerically checked that adding to such a solution $\mathbf{d}$, a constant multiple of the unit normal $\mathbf{n}$ yields another solution to (23). It is important to note that such a change has no influence on the flow velocity $\mathbf{u}$ given by (21) or on the force $\mathbf{F}$ and torque $\boldsymbol{\Gamma}$.

3. Asymptotic analysis for a distant and arbitrarily shaped particle

This key section presents the asymptotic analysis developed for a distant particle, i.e. when the distance d between the particle centre of mass O' and the upper porous slab boundary Σ_u is much larger than the particle characteristic length scale a.

3.1. Assumptions, ambient flow decomposition and asymptotic expansion of the Green tensor

For a distant particle, it is possible to invert the boundary-integral equation (23) using an asymptotic expansion in terms of the small parameter $\varepsilon = a/d \ll 1$. In (23) both points $\mathbf{x}$ and $\mathbf{y}$ are located on the particle surface S, which is far from the $x_3 = 0$ plane surface Σ_u.

Let $\mathbf{x}_c = d\mathbf{e}_3$ be the position of the particle centre of mass O'. Defining the positions $\mathbf{x}' = \mathbf{x} - d\mathbf{e}_3$ and $\mathbf{y}' = \mathbf{y} - d\mathbf{e}_3$ relative to O', we have $|\mathbf{x}'| = O(a) \ll d$ and $|\mathbf{y}'| = O(a) \ll d$ when both $\mathbf{x}$ and $\mathbf{y}$ lie on the particle surface S in (23). We then expand the ambient flow velocity $\mathbf{v}_\infty(\mathbf{x})$ and the Green tensor $\mathbf{G}(\mathbf{x},\mathbf{y})$ in terms of the small parameter ε for $\mathbf{x}$ and $\mathbf{y}$ located on the surface S, which is near O'. Recalling (9), we first have, using the link $x_3 = x_3' + d$,

$$\begin{aligned}\mathbf{v}_\infty(\mathbf{x}) = \gamma_2 d^2\left\{1 - \frac{2K}{a^2}\varepsilon^2 + 2(\frac{x_3'}{a})\varepsilon + (\frac{x_3'}{a})^2\varepsilon^2\right\}\mathbf{e}_1 \\ + \gamma_1 d\left\{1 + \frac{\sqrt{K}}{\sigma a}\varepsilon + (\frac{x_3'}{a})\varepsilon\right\}\mathbf{e}_1.\end{aligned} \tag{26}$$

By linearity, we then confine our attention to the three following ambient flows: an uniform flow $\mathbf{v}_\infty^u = \mathbf{e}_1$, a linear shear flow $\mathbf{v}_\infty^{ls} = (x_3'/a)\mathbf{e}_1$ and a quadratic shear flow $\mathbf{v}_\infty^{qs} = (x_3'/a)^2\mathbf{e}_1$. These flow velocities have a typical magnitude of order unity on the particle boundary.

From (18), it is also needed to expand each smooth component $R_{jk}(\mathbf{x},\mathbf{y})$ around O' as follows:

$$R_{jk}(\mathbf{x},\mathbf{y}) = R_{jk}(\mathbf{x}_c,\mathbf{x}_c) + [\boldsymbol{\nabla}_\mathbf{x} R_{jk}](\mathbf{x}_c,\mathbf{x}_c)\cdot\mathbf{x}' + [\boldsymbol{\nabla}_\mathbf{y} R_{jk}](\mathbf{x}_c,\mathbf{x}_c)\cdot\mathbf{y}' + \cdots \tag{27}$$

Note that in applying (27) we use the relationships $\partial/\partial x_\alpha = -\partial/\partial y_\alpha = \partial/\partial R'_\alpha$ for $\alpha = 1, 2$ and also $\partial/\partial x_3 = \partial/\partial y_3 = \partial/\partial R'_3$. Moreover, for $\mathbf{x} = \mathbf{y} = \mathbf{x}_c$, we have $\rho = 0$ and $R'_3 = 2d$ in (19). Inspecting (20) then shows that some derivatives (with respect to the variables R'_l) of transform $\langle g \rangle$ (recall (19)) must be evaluated at $\rho = 0$ for large $R'_3 = 2d$. This is achieved by exploiting the relationships

$$\left[\frac{\partial \langle g \rangle}{\partial R'_j}\right]_{\rho=0} = -\delta_{j3} \int_0^\infty g(\xi) \xi e^{-R'_3 \xi} \mathrm{d}\xi \quad \text{for } j = 1, 2, 3 \tag{28}$$

$$\left[\frac{\partial^2 \langle g \rangle}{\partial R'_j \partial R'_l}\right]_{\rho=0} = c_{jl} \int_0^\infty g(\xi) \xi^2 e^{-R'_3 \xi} \mathrm{d}\xi \quad \text{for } j, l = 1, 2, 3 \tag{29}$$

with $c_{jl} = (3\delta_{j3}\delta_{l3} - \delta_{jl})/2$, the additional identity

$$\left[\frac{\partial^3 \langle g \rangle}{\partial R'_i \partial R'_j \partial R'_l}\right]_{\rho=0} = d_{ijl} \int_0^\infty g(\xi) \xi^3 e^{-R'_3 \xi} \mathrm{d}\xi \tag{30}$$

and the definitions (valid for $i = 1, 2; j = 1, 2, 3$ and $l = 1, 2, 3$)

$$d_{ijl} = 0 \text{ if } j = l = 3 \text{ or } (j-3)(l-3) \neq 0, \tag{31}$$

$$d_{ijl} = -c_{ij} \text{ if } j \neq 3 \text{ and } l = 3, \tag{32}$$

$$d_{ijl} = -c_{il} \text{ if } j = 3 \text{ and } l \neq 3. \tag{33}$$

In evaluating the derivative $\partial R_{jk}/\partial y_3 = \partial R_{jk}/\partial R'_3$ for (27), note that both functions f_1 and f_4 (recall appendix A) also depend upon y_3! The expansion (27) of each component $R_{jk}(\mathbf{x}, \mathbf{y})$ is finally gained by appealing, for a function f that is smooth enough near the origin, to the following asymptotic approximation (see [14]):

$$\int_0^\infty f(t) e^{-\lambda t} \, \mathrm{d}t \sim \sum_{n=0}^{N} \frac{f^{(n)}(0)}{n!} \left[\int_0^\infty \mathrm{e}^{-u} u^n \mathrm{d}u\right] \lambda^{-(n+1)} \quad \text{as } \lambda \to \infty. \tag{34}$$

The manipulations, too long to be reproduced here, are illustrated in Appendix B for all terms involving the function f_1 (which depends upon y_3). From the decomposition (18) and the approximation (27), the desired expansion of the Green tensor $\mathbf{G}(\mathbf{x}, \mathbf{y})$ when both $\mathbf{x}$ and $\mathbf{y}$ lie on the distant particle surface is then found to write

$$\mathbf{G}(\mathbf{x}, \mathbf{y}) = \mathbf{G}^\infty(\mathbf{x}, \mathbf{y}) + \varepsilon \mathbf{G}^{(1)} + \varepsilon^2 \left[\mathbf{G}^{(2)} + \mathbf{W} \cdot \mathbf{y}' + \mathbf{L} \cdot \mathbf{x}'\right] + O(\varepsilon^3) \tag{35}$$

in which the *uniform* second-rank *diagonal* tensors $\mathbf{G}^{(1)}, \mathbf{G}^{(2)}$ and *uniform* third-rank tensors $\mathbf{W}$ and $\mathbf{L}$ have the following simple Cartesian components

$$G^{(1)}_{jk} = -\frac{3}{4a}[1 + \delta_{j3}]\delta_{kj}, \tag{36}$$

$$G^{(2)}_{jk} = \frac{3\sqrt{K}\delta_{jk}}{4a^2\sigma}\left[1 + \delta_{j3} + (1 + 5\delta_{j3})\frac{\sigma\sqrt{K}}{e}\right], \tag{37}$$

$$L_{jkl} = -W_{jkl} = \frac{3}{8a^2}\left[\delta_{j3}\delta_{kl} - \delta_{k3}\delta_{jl}\right] \quad \text{for } l = 1, 2 \tag{38}$$

$$W_{jk3} = L_{jk3} = \frac{3}{8a^2}[1 + \delta_{j3}]\delta_{kj}. \tag{39}$$

The key results (35)–(39) suggest the following basic comments:

(a) The slip coefficient σ and the lengths e and $\sqrt{K}$ appear only in $\mathbf{G}^{(2)}$. Hence, the approximation of the Green tensor at order $O(\varepsilon)$ is the same as the one of the Green tensor derived by [15] for an impermeable wall on which the no-slip condition applies. This indicates that the porous slab with Beavers and Joseph boundary conditions behaves at this order $O(\varepsilon)$ as a solid boundary Σ_u at rest for a distant particle located in the upper fluid.

(b) As a consequence of the previous remark (a), the resistance tensors $\mathbf{B}$ and $\mathbf{C}$ introduced by (15) are transposed at order $O(\varepsilon)$ whatever is the particle shape.

(c) For $\mathbf{x}$ and $\mathbf{y}$ on the particle surface $\mathbf{G}^{\infty}(\mathbf{x},\mathbf{y}) \sim 1/a, \mathbf{G}^{1} \sim 1/a, \mathbf{W}\cdot\mathbf{y}' \sim 1/a$ and $\mathbf{L}\cdot\mathbf{x}' \sim 1/a$. Under the assumptions

$$\sqrt{K} \leq O(e),\ \sqrt{K}/\sigma \leq O(a) \tag{40}$$

it is clear from (37) that also $\mathbf{G}^{2} \sim 1/a$ so that the asymptotic expansion (35) is consistent. Note that the reasonable assumptions (40) mean that the porous slab thickness e is, as mentioned in the "Introduction", at least of the order typical pore size $\sqrt{K}$ and also that the slab slip length $\sqrt{K}/\sigma$ is not larger than the particle length scale a.

3.2. Second-order solution for arbitrarily shaped distant particles

The required asymptotic solution of the key boundary-integral equation (23) is obtained using (35)–(39) and combining the results obtained by successively taking $\mathbf{u}_d = \mathbf{U} + \boldsymbol{\Omega}\wedge\mathbf{x}'$ with $\mathbf{U}$ and $\boldsymbol{\Omega}$ of unit magnitude, $\mathbf{u}_d = -\mathbf{v}^{u}_{\infty} = -\mathbf{e}_1, \mathbf{u}_d = -\mathbf{v}^{ls}_{\infty} = -(x'_3/a)\mathbf{e}_1$ or $\mathbf{u}_d = -\mathbf{v}^{qs}_{\infty} = -(x'_3/a)^2\mathbf{e}_1$. For each previous choice, the velocity $\mathbf{u}_d$ on the left-hand side of (23) is of unit magnitude on the particle surface, and the unknown surface density may be searched for as an asymptotic expansion

$$\mathbf{d}(\mathbf{y}) = \mathbf{d}_0(\mathbf{y}) + \varepsilon\mathbf{d}_1(\mathbf{y}) + \varepsilon^2\mathbf{d}_2(\mathbf{y}) + O(\varepsilon^3). \tag{41}$$

In the absence of gravity, the resulting force $\mathbf{F}$ and torque $\boldsymbol{\Gamma}$ experienced by the particle (invoking (22)) are then expressed as expansions:

$$\mathbf{F} = \mathbf{F}_0 + \varepsilon\mathbf{F}_1 + \varepsilon^2\mathbf{F}_2 + O(\varepsilon^3),\ \mathbf{F}_l = \int_S \mathbf{d}_l \mathrm{d}S\ \ (l = 0,1,2), \tag{42}$$

$$\boldsymbol{\Gamma} = \boldsymbol{\Gamma}_0 + \varepsilon\boldsymbol{\Gamma}_1 + \varepsilon^2\boldsymbol{\Gamma}_2 + O(\varepsilon^3),\ \boldsymbol{\Gamma}_l = \int_S \mathbf{x}'\wedge\mathbf{d}_l \mathrm{d}S\ \ (l = 0,1,2). \tag{43}$$

Defining the linear operator $\mathcal{L}$ with

$$\mathcal{L}[\mathbf{d}] = -\frac{1}{8\pi\mu}\int_S \mathbf{G}^{\infty}(\mathbf{x},\mathbf{y})\cdot\mathbf{d}(\mathbf{y})\mathrm{d}S, \tag{44}$$

the leading term $\mathbf{d}_0(\mathbf{y})$ is readily seen to satisfy

$$\mathcal{L}[\mathbf{d}_0] = -\frac{1}{8\pi\mu}\int_S \mathbf{G}^{\infty}(\mathbf{x},\mathbf{y})\cdot\mathbf{d}_0(\mathbf{y})\mathrm{d}S = \mathbf{u}_d(\mathbf{x})\ \text{ for } \mathbf{x} \text{ on } S. \tag{45}$$

and the resulting force $\mathbf{F}_0$ and torque $\boldsymbol{\Gamma}_0$ read

$$\mathbf{F}_0 = \int_S \mathbf{d}_0 \mathrm{d}S,\ \boldsymbol{\Gamma}_0 = \int_S \mathbf{x}'\wedge\mathbf{d}_0 \mathrm{d}S. \tag{46}$$

It should be noted that (45) admits, provided that $\int_S \mathbf{u}_d\cdot\mathbf{n}\mathrm{d}S = 0$, a solution $\mathbf{d}_0$ defined up to a constant multiple of the normal $\mathbf{n}$, which has no influence on the values of $\mathbf{F}_0$ and $\boldsymbol{\Gamma}_0$. Moreover, the result (45) suggests distinguishing two different circumstances:

(a) The case of a rigid-body motion $\mathbf{u}_d = \mathbf{U}+\boldsymbol{\Omega}\wedge\mathbf{x}'$. This occurs either in Case (i) or for the contribution of a uniform ambient flow that is $\mathbf{v}^u_\infty = \mathbf{e}_1$ in the treatment of Case (ii) (taking then $\boldsymbol{\Omega} = \mathbf{0}$ and $\mathbf{U} = -\mathbf{e}_1$). It then turns out (see [16]) that (45) is the boundary-integral equation governing the surface traction $\mathbf{f}_0$ arising on the boundary of the particle when it experiences this rigid-body motion in an *unbounded fluid*. In other words, $\mathbf{d}_0 = \mathbf{f}_0$ (up to a constant multiple of $\mathbf{n}$) for a particle experiencing a rigid-body motion.

One can retain the solution $\mathbf{f}_0$ reading $\mathbf{f}_0 = \mu\{\mathbf{T}^t_0 \cdot \mathbf{U} + \mathbf{T}^r_0 \cdot \boldsymbol{\Omega}\}$ with second-rank tensors $\mathbf{T}^t_0$ and $\mathbf{T}^r_0$ determined by successively solving (45) for $\mathbf{u}_d = \mathbf{U}$ and $\mathbf{u}_d = \boldsymbol{\Omega} \wedge \mathbf{x}'$. In addition, the associated resistance tensors (recall (15)) $\mathbf{A}_0, \mathbf{B}_0, \mathbf{C}_0$ and $\mathbf{D}_0$ are such that $\mathbf{B}_0$ and $\mathbf{C}_0$ are each other's transposed so that

$$\mathbf{F}_0 = -\mu\{\mathbf{A}_0 \cdot \mathbf{U} + \mathbf{B}_0 \cdot \boldsymbol{\Omega}\},\ \boldsymbol{\Gamma}_0 = -\mu\{{}^t\mathbf{B}_0 \cdot \mathbf{U} + \mathbf{D}_0 \cdot \boldsymbol{\Omega}\}. \tag{47}$$

(b) Whenever $\mathbf{u}_d$ is not a rigid-body motion (here in Case (ii) for $\mathbf{u}_d = -\mathbf{v}^{ls}_\infty$ or $\mathbf{u}_d = -\mathbf{v}^{qs}_\infty$) the density $\mathbf{d}_0$ is not any more equal (up to a constant multiple of $\mathbf{n}$) to the surface traction $\mathbf{f}_0$ arising on the particle surface when it is held fixed in an unbounded fluid in the ambient velocity field $\mathbf{v}^{ls}_\infty$ or $\mathbf{v}^{qs}_\infty$. Actually, the integral representation of the disturbance velocity $\mathbf{u}$ in an unbounded fluid now involves both the single-layer term (with tensor $\mathbf{G}^\infty$) and also a double-layer term.

The first-order density $\mathbf{d}_1$ is immediately seen to obey the boundary-integral equation

$$\mathcal{L}[\mathbf{d}_1] = \frac{1}{8\pi\mu}\mathbf{G}^{(1)} \cdot \mathbf{F}_0 \ \text{ for } \mathbf{x} \text{ on } S. \tag{48}$$

Since the right-hand side of (48) is uniform, the solution (up to a constant times $\mathbf{n}$) is

$$\mathbf{d}_1 = \frac{1}{8\pi}\mathbf{T}^t_0 \cdot (\mathbf{G}^{(1)} \cdot \mathbf{F}_0) \tag{49}$$

and the resulting identities hold

$$\mathbf{F}_1 = -\frac{1}{8\pi}\mathbf{A}_0 \cdot (\mathbf{G}^{(1)} \cdot \mathbf{F}_0),\ \boldsymbol{\Gamma}_1 = -\frac{1}{8\pi}\ {}^t\mathbf{B}_0 \cdot (\mathbf{G}^{(1)} \cdot \mathbf{F}_0). \tag{50}$$

Finally, the second-order density $\mathbf{d}_2$ is governed by the boundary-integral equation

$$\mathcal{L}[\mathbf{d}_2] = \frac{1}{8\pi\mu}\Big\{(\mathbf{L} \cdot \mathbf{x}') \cdot \int_S \mathbf{d}_0 \mathrm{d}S + \mathbf{G}^{(1)} \cdot \int_S \mathbf{d}_1 \mathrm{d}S + \mathbf{G}^{(2)} \cdot \int_S \mathbf{d}_0 \mathrm{d}S + \int_S (\mathbf{W} \cdot \mathbf{y}') \cdot \mathbf{d}_0 \mathrm{d}S\Big\} \ \text{ for } \mathbf{x} \text{ on } S. \tag{51}$$

Note that using the definitions (38)–(39) easily shows that the right-hand side $\mathbf{u}_2$ of (51) satisfies the compatibility relation $\int_S \mathbf{u}_2 \cdot \mathbf{n}\mathrm{d}S = 0$. Moreover, the first term on the right-hand side of (51) linearly depends upon the vector $\mathbf{x}'$. As usual, it is decomposed as a pure straining motion and a pure rotation. That is, we

$$(\mathbf{L} \cdot \mathbf{x}') \cdot \int_S \mathbf{d}_0 \mathrm{d}S = (\mathbf{L} \cdot \mathbf{x}') \cdot \mathbf{F}_0 = \mu\big\{\mathbf{E}^{(2)} \cdot \mathbf{x}' + \boldsymbol{\Omega}^{(2)} \wedge \mathbf{x}'\big\} \tag{52}$$

with, denoting by ϵ_{ijk} the usual Levi–Civita permutation tensor components, the following Cartesian components of the so-called rate-of-strain tensor $\mathbf{E}^{(2)}$ and angular velocity $\boldsymbol{\Omega}^{(2)}$

$$E^{(2)}_{jl} = \frac{1}{2\mu}(L_{jkl} + L_{lkj})(\mathbf{F}_0 \cdot \mathbf{e}_k),\ \Omega^{(2)}_i = \frac{1}{4\mu}\epsilon_{ijl}(L_{lkj} - L_{jkl})(\mathbf{F}_0 \cdot \mathbf{e}_k). \tag{53}$$

Appealing to (38) shows that $\boldsymbol{\Omega}^{(2)} = \mathbf{0}$. One thus solely needs to determine the density $\mathbf{d}_{st}$ obtained when the particle is held fixed (in an unbounded domain) in the external pure straining velocity field $-\mathbf{E}^{(2)} \cdot \mathbf{x}'$.

Hence, $\mathbf{d}_{st}$ is solution to the linear equation $\mathcal{L}[\mathbf{d}_{st}] = \mathbf{E}^{(2)} \cdot \mathbf{x}'$ with $\mathbf{E}^{(2)}$ linear in $\mathbf{F}_0$. Consequently, $\mathbf{d}_{st} = \mathbf{T}_0^{st} \cdot \mathbf{F}_0$ with $\mathbf{T}_0^{st}$ a shape-dependent second-rank tensor. Going back to (51), it follows that

$$\mathbf{d}_2 = \frac{1}{8\pi}\Bigg\{\mathbf{T}_0^{st} \cdot \mathbf{F}_0 + \mathbf{T}_0^{t} \cdot \left[\mathbf{G}^{(1)} \cdot \mathbf{F}_1 + \mathbf{G}^{(2)} \cdot \mathbf{F}_0 + \int_S (\mathbf{W} \cdot \mathbf{y}') \cdot \mathbf{d}_0 \mathrm{d}S\right]\Bigg\} \tag{54}$$

and therefore also that

$$\mathbf{F}_2 = \frac{1}{8\pi}\Bigg\{\left[\int_S \mathbf{T}_0^{st} \mathrm{d}S\right] \cdot \mathbf{F}_0 - \mathbf{A}_0 \cdot \left[\mathbf{G}^{(1)} \cdot \mathbf{F}_1 + \mathbf{G}^{(2)} \cdot \mathbf{F}_0 + \int_S (\mathbf{W} \cdot \mathbf{y}') \cdot \mathbf{d}_0 \mathrm{d}S\right]\Bigg\}, \tag{55}$$

$$\mathbf{\Gamma}_2 = \frac{1}{8\pi}\Bigg\{\left[\int_S \mathbf{x}' \wedge (\mathbf{T}_0^{st} \cdot \mathbf{F}_0) \mathrm{d}S\right] - {}^t\mathbf{B}_0 \cdot \left[\mathbf{G}^{(1)} \cdot \mathbf{F}_1 + \mathbf{G}^{(2)} \cdot \mathbf{F}_0 + \int_S (\mathbf{W} \cdot \mathbf{y}') \cdot \mathbf{d}_0 \mathrm{d}S\right]\Bigg\}. \tag{56}$$

In summary, the asymptotic expansions (42)–(43) for a distant and arbitrarily shaped particle require to evaluate a few quantities obtained when the particle is suspended in *an unbounded fluid:* the density $\mathbf{d}_0$ and the second-rank tensors $\mathbf{A}_0, \mathbf{B}_0, \mathbf{T}_0^{st}$. As previously noticed, $\mathbf{d}_0, \mathbf{d}_1$ and $\mathbf{d}_2$ are obtained up to a constant multiple of the unit normal vector $\mathbf{n}$. As expected, the resulting net force, net torque, vector (see Appendix C) $\int_S (\mathbf{W} \cdot \mathbf{y}') \cdot \mathbf{d}_0 \mathrm{d}S$ and therefore right-hand sides of (48), (50)–(51) and (54)–(56) are not affected by the selected constants multiple of the unit normal vector.

In general, a numerical procedure is needed to determine those quantities. It should also be noted that the porous slab properties (e, K, σ) solely affect the second-order terms $\mathbf{F}_2, \mathbf{\Gamma}_2$ and $\mathbf{d}_2$ through the vector $\mathbf{G}^{(2)} \cdot \mathbf{F}_0$ in (54)–(56).

4. Analytical treatment for a distant spherical particle

For a spherical particle, it is possible to derive analytical expressions for the different terms entering in the previous asymptotic approximations.

4.1. Rigid-body motion and settling migration of a distant sphere

For a sphere with radius a and centre O' experiencing a rigid-body motion with velocity $\mathbf{u}_d = \mathbf{U} + \mathbf{\Omega} \wedge \mathbf{x}'$ on its surface, the resulting surface traction $\mathbf{f}_0$ is such that [17]

$$\mathbf{f}_0 = \mathbf{d}_0 = -\frac{3\mu}{2a}[\mathbf{U} + 2\mathbf{\Omega} \wedge \mathbf{x}'], \ \mathbf{F}_0 = -6\pi\mu a \mathbf{U}, \ \mathbf{\Gamma}_0 = -8\pi\mu a^3 \mathbf{\Omega}. \tag{57}$$

Deriving $\mathbf{d}_1$ is straightforward. As shown previously, in obtaining $\mathbf{d}_2$ we need to consider a Stokes flow about the sphere with velocity $\mathbf{v}$ defined as

$$\mathbf{v}(\mathbf{x}) = -\frac{1}{8\pi\mu}\int_S \mathbf{G}^{\infty}(\mathbf{x}, \mathbf{y}) \cdot \mathbf{d}_{st}(\mathbf{y}) \mathrm{d}S(\mathbf{y}) \quad \text{for } |\mathbf{x}'| \geq a \tag{58}$$

and taking the value $\mathbf{E}^{(2)}\cdot\mathbf{x}'$ on the sphere surface. Invoking the usual Faxen relations [18] for a sphere immediately shows that such a flow exerts on the sphere a force $\mathbf{F}_{st}$ and a torque $\mathbf{\Gamma}_{st}$ given by

$$\mathbf{F}_{st}=-\frac{3\mu}{2a}\int\limits_S \mathbf{E}^{(2)}\cdot\mathbf{x}\mathrm{d}S,\ \mathbf{\Gamma}_{st}=-\frac{3\mu}{a}\int\limits_S \mathbf{x}'\wedge\mathbf{E}^{(2)}\cdot\mathbf{x}\mathrm{d}S. \tag{59}$$

Symmetries and the definition (53) of $\mathbf{E}^{(2)}$ give $\mathbf{F}_{st}=\mathbf{\Gamma}_{st}=\mathbf{0}$ so that the first term on the right-hand side of (55) and (56) vanishes. As the reader may easily check, using (57) and the definitions (38)–(39) also easily yields

$$\int\limits_S(\mathbf{W}\cdot\mathbf{y}')\cdot\mathbf{d}_0(\mathbf{y}')\mathrm{d}S=\mathbf{0}. \tag{60}$$

Elementary manipulations then provide the following asymptotic expansions:

$$\begin{aligned}\mathbf{F}=&-6\pi\mu a\Big\{\mathbf{U}+\frac{9\varepsilon}{16}\Big[(\mathbf{U}\cdot\mathbf{e}_1)\mathbf{e}_1+(\mathbf{U}\cdot\mathbf{e}_2)\mathbf{e}_2+2(\mathbf{U}\cdot\mathbf{e}_3)\mathbf{e}_3\Big]\\&+\frac{9\varepsilon^2}{16}\Big[\Big[\frac{9}{16}-\frac{\sqrt{K}}{a\sigma}(1+\sigma\sqrt{K}/e)\Big]\big[(\mathbf{U}\cdot\mathbf{e}_1)\mathbf{e}_1+(\mathbf{U}\cdot\mathbf{e}_2)\mathbf{e}_2\big]\\&+\Big[\frac{9}{4}-\frac{2\sqrt{K}}{a\sigma}(1+3\sigma\sqrt{K}/e)\Big](\mathbf{U}\cdot\mathbf{e}_3)\mathbf{e}_3\Big]\Big\}\\&+O\left(a^3\mu|\mathbf{\Omega}|\varepsilon^3,a^2\mu|\mathbf{U}|\varepsilon^3\right),\end{aligned} \tag{61}$$

$$\mathbf{\Gamma}=-8\pi\mu a^3\mathbf{\Omega}+O\left(a^3\mu|\mathbf{\Omega}|\varepsilon^3,a^2\mu|\mathbf{U}|\varepsilon^3\right). \tag{62}$$

Inspecting (61)–(62) readily gives the asymptotic expansions of the resistance tensors $\mathbf{A},\mathbf{B},\mathbf{C}$ and $\mathbf{D}$ introduced by (15). Here we note that at the retained order of approximation, $\mathbf{B}={}^t\mathbf{C}=\mathbf{0}$. For further comparisons achieved in §4.3, we also cast (61)–(62) into the following forms (of course summing indices i in (63)–(64))

$$\mathbf{F}=-6\pi\mu a[1+f_1^{(i)}\varepsilon+f_2^{(i)}\varepsilon^2](\mathbf{U}\cdot\mathbf{e}_i)\mathbf{e}_i+O\left(a^3\mu|\mathbf{\Omega}|\varepsilon^3,a^2\mu|\mathbf{U}|\varepsilon^3\right), \tag{63}$$

$$\mathbf{\Gamma}=-8\pi\mu a^3[1+c_1^{(i)}\varepsilon+c_2^{(i)}\varepsilon^2](\mathbf{\Omega}\cdot\mathbf{e}_i)\mathbf{e}_i+O\left(a^3\mu|\mathbf{\Omega}|\varepsilon^3,a^2\mu|\mathbf{U}|\varepsilon^3\right), \tag{64}$$

with the coefficients

$$f_1^{(1)}=f_1^{(2)}=f_1^{(3)}/2=\frac{9}{16},\ c_1^{(i)}=c_1^{(i)}=0\text{ for }i=1,2,3, \tag{65}$$

$$f_2^{(1)}=f_2^{(2)}=\frac{9}{16}\left[\frac{9}{16}-\frac{\sqrt{K}}{a\sigma}(1+\sigma\sqrt{K}/e)\right], \tag{66}$$

$$f_2^{(3)}=\frac{9}{16}\left[\frac{9}{4}-\frac{2\sqrt{K}}{a\sigma}(1+3\sigma\sqrt{K}/e)\right]. \tag{67}$$

In addition, exploiting (16) then shows that a distant sphere with uniform density ρ_s settles with translational velocity $\mathbf{U}_s$ and angular velocity $\mathbf{\Omega}_s$ given by

$$\begin{aligned}\mathbf{U}_s=&\frac{2a^2}{9\mu}(\rho_s-\rho_f)\Big\{\mathbf{g}-\frac{9\varepsilon}{16}\left[(\mathbf{g}\cdot\mathbf{e}_1)\mathbf{e}_1+(\mathbf{g}\cdot\mathbf{e}_2)\mathbf{e}_2+2(\mathbf{g}\cdot\mathbf{e}_3)\mathbf{e}_3\right]\\&+\frac{9\varepsilon^2}{16}\Big(\frac{\sqrt{K}}{a\sigma}\Big)\left[\left(1+\frac{\sigma\sqrt{K}}{e}\right)\left[(\mathbf{g}\cdot\mathbf{e}_1)\mathbf{e}_1+(\mathbf{g}\cdot\mathbf{e}_2)\mathbf{e}_2\right]+2\left(1+3\frac{\sigma\sqrt{K}}{e}\right)(\mathbf{g}\cdot\mathbf{e}_3)\mathbf{e}_3\right]+O(\varepsilon^3\mathbf{g})\Big]\Big\},\end{aligned} \tag{68}$$

$$\mathbf{\Omega}_s=O(\varepsilon^3a|\rho_s-\rho_f||\mathbf{g}|/\mu). \tag{69}$$

4.2. Results for a distant sphere held fixed in a linear or quadratic ambient shear flow

This subsection considers a distant sphere ($\varepsilon = a/d \ll 1$) *held fixed*, in the absence of gravity, in the ambient flow Stokes flow $(\mathbf{v}_\infty, q_\infty)$ given by (9). We search for the force $\mathbf{F}_a$ and torque $\mathbf{\Gamma}_a$ (about the sphere centre O') experienced by the sphere. For $\varepsilon = 0$, these vectors, denoted by $\mathbf{F}_a^\infty$ and $\mathbf{\Gamma}_a^\infty$, are easily obtained by using the so-called Faxen relations [18] for a sphere and read

$$\mathbf{F}_a^\infty = 6\pi\mu a \left\{ \gamma_1 \left[d + \frac{\sqrt{K}}{\sigma} \right] + \gamma_2 \left[d^2 - 2K + \frac{a^2}{3} \right] \right\} \mathbf{e}_1, \tag{70}$$

$$\mathbf{\Gamma}_a^\infty = 8\pi\mu a^3 \left\{ \frac{\gamma_1}{2} + \gamma_2 d \right\} \mathbf{e}_2. \tag{71}$$

For $\varepsilon > 0$ symmetries show that $\mathbf{F}_a \wedge \mathbf{e}_1 = \mathbf{\Gamma}_a \wedge \mathbf{e}_2 = \mathbf{0}$. Taking account of (70)–(71), we then write the net force $\mathbf{F}_a^l$ and net torque $\mathbf{\Gamma}_a^l$ exerted on the sphere by a *pure linear* ambient shear flow (take $\gamma_2 = 0$) as

$$\mathbf{F}_a^l = 6\pi\mu a\gamma_1 \left[d + \frac{\sqrt{K}}{\sigma} \right] f^l \mathbf{e}_1, \ \mathbf{\Gamma}_a^l = 4\pi\mu a^3 \gamma_1 c^l \mathbf{e}_2 \tag{72}$$

introducing the force and torque friction coefficients f^l and c^l. Similarly, a *pure quadratic* ambient shear flow (obtained for $\gamma_1 = 0$) applies on the sphere a force $\mathbf{F}_a^q$ and torque $\mathbf{\Gamma}_a^q$ in the form

$$\mathbf{F}_a^q = 6\pi\mu a\gamma_2 \left[d^2 - 2K + \frac{a^2}{3} \right] f^q \mathbf{e}_1, \ \mathbf{\Gamma}_a^q = 8\pi\mu a^3 \gamma_2 d c^q \mathbf{e}_2 \tag{73}$$

with friction coefficients f^q and c^q. The quantities f^l, c^l, f^q and c^q depend upon $(\sigma, \sqrt{K}/a, e/a)$ and the small separation parameter $\varepsilon = a/d$. Moreover, each friction coefficient tends to unity as ε vanishes. From the asymptotic analysis developed in §3, we therefore write for the distant sphere

$$f^l = 1 + f_1^l\varepsilon + f_2^l\varepsilon^2 + O(\varepsilon^3), \ c^l = 1 + c_1^l\varepsilon + c_2^l\varepsilon^2 + O(\varepsilon^3), \tag{74}$$

$$f^q = 1 + f_1^q\varepsilon + f_2^q\varepsilon^2 + O(\varepsilon^3), \ c^q = 1 + c_1^q\varepsilon + c_2^q\varepsilon^2 + O(\varepsilon^3) \tag{75}$$

in terms of eight constants $f_1^l, \ldots, c_2^q$ to be analytically determined using §3.2. From the decomposition (26), this task reduces to three cases: $\mathbf{u}_d = -\mathbf{e}_1$ (already done using (61)–(62) and thus not repeated here), $\mathbf{u}_d = -(x_3'/a)\mathbf{e}_1$ and $\mathbf{u}_d = -(x_3'/a)^2\mathbf{e}_1$. For those two latter flows, the material in §3.2 is used after noting that the relations (47) with $\mathbf{d}_0$ solution to (45) *for the sphere with radius a* become

$$\mathbf{F}_0 = -\frac{3\mu}{2a} \int_S \mathbf{u}_d \mathrm{d}S, \ \mathbf{\Gamma}_0 = -\frac{3\mu}{a} \int_S \mathbf{x}' \wedge \mathbf{u}_d \mathrm{d}S. \tag{76}$$

As the reader may easily check, the force $\mathbf{F}_a^{ls}$ and torque $\mathbf{\Gamma}_a^{ls}$ experienced by the sphere *held fixed* in the ambient flow $(x_3'/a)\mathbf{e}_1$ then satisfy

$$\mathbf{F}_a^{ls} = 6\pi\mu a O(\varepsilon^3)\mathbf{e}_1, \ \mathbf{\Gamma}_a^{ls} = 4\pi\mu a^3[1 + O(\varepsilon^3)]\mathbf{e}_2. \tag{77}$$

In a similar fashion, the net force $\mathbf{F}_a^{qs}$ and torque $\mathbf{\Gamma}_a^{qs}$ exerted on a motionless sphere by the ambient flow $(x_3'/a)^2\mathbf{e}_1$ read

$$\mathbf{F}_a^{qs} = 2\pi\mu \left\{ 1 + \frac{9\varepsilon}{16} + \frac{9\varepsilon^2}{16} \left[\frac{9}{16} - \frac{\sqrt{K}}{a\sigma}(1 + \sigma\sqrt{K}/e) \right] + O(\varepsilon^3) \right\} \mathbf{e}_1$$
$$- \frac{3a}{4} \left[\int_S (\mathbf{W} \cdot \mathbf{y}') \cdot \mathbf{d}_0(\mathbf{y}') \mathrm{d}S \right] \varepsilon^2, \tag{78}$$

$$\mathbf{\Gamma}_a^{qs} = O(\mu a^3 \varepsilon^3)\mathbf{e}_2. \tag{79}$$

Note that for the imposed ambient quadratic shear flow, symmetries show that it is possible to retain a solution $\mathbf{d}_0$ to (45) such that $\mathbf{d}_0(\mathbf{y}') = \mathbf{d}_0(-\mathbf{y}')$ at any point $\mathbf{y}'$ on the sphere's surface. Accordingly, the last term on the right-hand side of (78) vanishes. Gathering the previous results and recalling the decomposition (26) then finally yields the required estimates (74)–(75). Our final results are

$$f^l = f^q = 1 + \frac{9\varepsilon}{16} + \frac{9\varepsilon^2}{16}\left[\frac{9}{16} - \frac{\sqrt{K}}{a\sigma}(1 + \sigma\sqrt{K}/e)\right] + O(\varepsilon^3), \tag{80}$$

$$c^l = c^q = 1 + O(\varepsilon^3). \tag{81}$$

It follows that

$$f_1^l = f_1^q = \frac{9}{16},\ c_1^l = c_1^q = c_2^l = c_2^q = 0, \tag{82}$$

$$f_2^l = f_2^q = \frac{9}{16}\left[\frac{9}{16} - \frac{\sqrt{K}}{a\sigma}(1 + \sigma\sqrt{K}/e)\right]. \tag{83}$$

Note that quantities $\sigma, \sqrt{K}/a$ and e/a solely appear in the second-order coefficients $f_2^l = f_2^q$.

4.3. Comparisons

In this section basic comparisons are made with asymptotic results available in the literature. In addition, the numerical predictions obtained by the boundary element approach implemented in [1] are checked against these asymptotic results.

4.3.1. Comparisons for a plane impermeable slipping wall. Asymptotic results for a sphere distant from a solid, impermeable wall on which a Navier slip boundary condition with slip length λ holds have been recently obtained for both a linear [13] and a quadratic [11] ambient shear flow (results for a no-slip wall were previously obtained in [12] and [19]). Using our previous notation (63)–(64) and (72)–(73), those results read for $\mathbf{U} \wedge \mathbf{e}_1 = \boldsymbol{\Omega} \wedge \mathbf{e}_2 = \mathbf{0}$

$$\mathbf{F} = -6\pi\mu a\left\{1 + \frac{9\varepsilon}{16} + \frac{9}{16}\left(\frac{9}{16} - \frac{\lambda}{a}\right)\varepsilon^2 + O(\varepsilon^3)\right\}\mathbf{U}, \tag{84}$$

$$\boldsymbol{\Gamma} = -8\pi\mu a^3[1 + O(\varepsilon^3)]\boldsymbol{\Omega} \tag{85}$$

and also

$$\mathbf{F}_a^l = 6\pi\mu a\gamma_1(d + \lambda)[1 + \frac{9\varepsilon}{16} + \frac{9}{16}\left(\frac{9}{16} - \frac{\lambda}{a}\right)\varepsilon^2 + O(\varepsilon^3)]\mathbf{e}_1, \tag{86}$$

$$\boldsymbol{\Gamma}_a^l = 4\pi\mu a^3\gamma_1[1 + O(\varepsilon^3)]\mathbf{e}_2, \tag{87}$$

$$\mathbf{F}_a^q = 6\pi\mu a\gamma_2 d^2[1 + \frac{9\varepsilon}{16} + \left(\frac{499}{768} - \frac{9\lambda}{16a}\right)\varepsilon^2 + O(\varepsilon^3)]\mathbf{e}_1, \tag{88}$$

$$\boldsymbol{\Gamma}_a^q = 8\pi\mu a^3\gamma_2 d[1 + O(\varepsilon^3)]\mathbf{e}_2. \tag{89}$$

As mentioned in the "Introduction", the case of a solid, impermeable wall with a Navier slip boundary condition and slip length λ is retrieved from the analysis developed in the present paper by taking $\sigma = \sqrt{K}/\lambda$ and letting $\sqrt{K}$ vanish. As the reader may check, using these choices when applying (63)–(67), (73)–(75) and (80)–(83) makes it possible to easily retrieve (84)–(89).

4.3.2. Comparisons for a porous slab. For our porous slab with thickness e and boundaries on which the Beavers and Joseph boundary conditions (7)–(8) apply, it is possible to confirm, for a distant sphere, the validity of the numerical results obtained by the indirect boundary formulation presented in [1]. This

TABLE 1. *Computed (using 4098 nodal points on the sphere surface) and theoretical (i.e. from the present asymptotic analysis) coefficients for a distant sphere with radius a and a porous slab with thickness e = a, coefficient σ = 1, 2 and normalized permeability K* = K/a² = 10⁻⁴*

	σ	$K^* = 10^{-4}$			
		$k = 1$	exact $k = 1$	$k = 2$	exact $k = 2$
$f_k^{(1)}$	1	0.5624	0.5625	0.3104	0.3107
$f_k^{(1)}$	2	0.5624	0.5625	0.3133	0.3135
$f_k^{(3)}$	1	1.1248	1.1250	1.2556	1.2540
$f_k^{(3)}$	2	1.1248	1.1250	1.2613	1.2597
$c_k^{(2)}$	1	1.1E−6	0	7.6E−4	0
$c_k^{(2)}$	2	7.2E−7	0	7.6E−4	0
$c_k^{(3)}$	1	6.9E−5	0	7.2E−4	0
$c_k^{(3)}$	2	6.9E−5	0	7.2E−4	0
f_k^l	1	0.5624	0.5625	0.3105	0.3107
f_k^l	2	0.5624	0.5625	0.3105	0.313
c_k^l	1	1.1E−5	0	0.0060	0
c_k^l	2	1.1E−5	0	0.0061	0
f_k^q	1	0.5624	0.5625	0.3110	0.3107
f_k^q	2	0.5624	0.5625	0.3138	0.3135
c_k^q	1	4.5E−6	0	0.0034	0
c_k^q	2	4.2E−6	0	0.0035	0

earlier work numerically inverts the boundary-integral equation (23) by employing a collocation boundary element technique. This is done here by using on the distant sphere's surface a $N-$node mesh made of curved 6-node triangular boundary elements. The procedure adopted for our comparisons is illustrated below for the force friction coefficients f_1^l and f_2^l (recall (72) and (74)). These coefficients obey

$$f_1^l = \lim_{\varepsilon \to 0} g_1^l(\varepsilon),\ g_1^l(t) = \frac{f^l(t) - 1}{t}, \tag{90}$$

$$f_2^l = \lim_{\varepsilon \to 0} g_2^l(\varepsilon),\ g_2^l(t) = \frac{f^l(t) - 1 - f_1^l t}{t^2}. \tag{91}$$

In practice, the function g_k^l is first calculated for several small values of $t > 0$, and the results are extrapolated to the required value at $t = 0$ by employing cubic splines. Here four values $t_1 = 1/8, t_2 = 1/9, t_3 = 1/10$ and $t_4 = 1/20$ have been used when evaluating the first-order term f_1^l, while three values $t_1 = 1/8, t_2 = 1/9$ and $t_3 = 1/10$ are employed for the second-order term f_2^l. The results presented in Tables 1 and 2 were obtained by distributing $N = 4098$ nodal points on the sphere surface. They concern the coefficients $f_1^{(1)}, f_2^{(1)}, f_1^{(3)}, f_2^{(3)}, c_1^{(2)}, c_2^{(2)}, c_1^{(3)}, c_2^{(3)}$ and $f_1^l, f_2^l, c_1^l, c_2^l, f_1^q, f_2^q, c_1^q, c_2^q$ for a porous slab with thickness $e = a$ and coefficient $\sigma = 1, 2$. Values of the normalized permeability $K^* = K/a^2$ are 10^{-4} and 10^{-2} in Tables 1 and 2, respectively.

As observed in these Tables, the numerical results obtained by using the indirect boundary-integral formulation developed in [1] perfectly agree with the asymptotic estimates.

TABLE 2. *Same as in Table 1 but for a normalized permeability* $K^* = K/a^2 = 10^{-2}$

	σ	$K^* = 10^{-2}$			
		$k = 1$	exact $k = 1$	$k = 2$	exact $k = 2$
$f_k^{(1)}$	1	0.5624	0.5625	0.2541	0.2545
$f_k^{(1)}$	2	0.5624	0.5625	0.2823	0.2827
$f_k^{(3)}$	1	1.1249	1.1250	1.1200	1.1194
$f_k^{(3)}$	2	1.1249	1.1250	1.1764	1.1756
$c_k^{(2)}$	1	6.4E−6	0	8.4E−4	0
$c_k^{(2)}$	2	4.0E−6	0	8.0E−4	0
$c_k^{(3)}$	1	6.8E−5	0	7.3E−4	0
$c_k^{(3)}$	2	6.8E−5	0	7.2E−4	0
f_k^l	1	0.5624	0.5625	0.2542	0.2545
f_k^l	2	0.5624	0.5625	0.2824	0.2827
c_k^l	1	2.3E−5	0	−0.0066	0
c_k^l	2	1.8E−5	0	−0.0059	0
f_k^q	1	0.5624	0.5625	0.2548	0.2545
f_k^q	2	0.5624	0.5625	0.2830	0.2827
c_k^q	1	1.0E−5	0	−0.0029	0
c_k^q	2	7.3E−6	0	−0.0026	0

5. Conclusions

A second-order asymptotic theory has been developed to quickly estimate the net force and torque experienced by a solid and arbitrarily shaped particle sufficiently distant from a porous slab and either held fixed in a shear flow or experiencing a prescribed rigid-body migration in a quiescent fluid. At each order, the task reduces to the solution on the particle's surface of a boundary-integral equation having for second-rank kernel tensor the classical Oseen–Burgers tensor. This is very different from the case of a solid particle at any distance from the porous slab for which, as proposed in [1], one has to invert on the particle surface a boundary-integral equation with a much more complicated tensor kernel. Because of the simple form of the Oseen–Burgers tensor, each boundary-integral equation encountered in the proposed asymptotic theory receives either a quick analytical (for a spherical particle, as achieved in the present paper) or numerical treatment (for a non-spherical particle). The asymptotic analysis shows that the porous slab thickness e, permeability K and associated slip length $\sqrt{K}/\sigma$ do not enter the first-order corrections to the solution prevailing in the absence of the slab. Actually, at the first order of approximation, the distant slab behaves for the particle as a solid, plane and no-slip wall. In other words, the slab properties $(e, K, \sqrt{K}/\sigma)$ play a role solely for the second-order corrections. Finally, one should note that the resulting and proposed asymptotic predictions for a distant sphere provide an excellent supplementary check for the numerical results obtained using the complicated boundary-integral equation in [1].

Appendix A

This Appendix defines the functions $f_1, \ldots, f_7$ that appear in (20). Such functions depend not only upon the porous slab length e, permeability $K > 0$ and dimensionless slip coefficient $\sigma > 0$ but also upon the location of the source point $\mathbf{y}$ through the quantity $y_3 = \mathbf{y} \cdot \mathbf{e}_3 > 0$. Upon introducing the quantities

$$\eta = \frac{\sqrt{K}}{\sqrt{K}\xi + \sigma}, \quad \tau = \frac{2K\xi}{\tanh(e\xi)}, \quad \tau' = \frac{2K\xi}{\sinh(e\xi)}, \tag{92}$$

$$\theta = 1 + 2\sigma\sqrt{K}\xi, \quad \Lambda = [1 + \xi(\tau + \theta\eta)]^{-1}, \quad S = (\xi\Lambda\tau')^2 \tag{93}$$

these functions indeed read

$$f_1 = \frac{2\Lambda}{1-S}[(\eta\xi - 1)y_3 - 2\eta], \ f_2 = \frac{2\Lambda}{S-1}[2\eta(1 + \sigma\sqrt{K}\xi) + \tau], \ f_5 = \eta f_2, \tag{94}$$

$$f_4 = \frac{2\Lambda\eta}{1-S}[(\xi y_3 - 2)\eta - y_3], \ f_3 = \frac{2S}{S-1}, \ f_6 = \eta f_3, \ f_7 = -\frac{2}{\sqrt{K}\xi + \sigma}. \tag{95}$$

Appendix B

This Appendix derives the contribution of the terms involving the function f_1 in (20) to the asymptotic expansion (27) of the quantity $R_{jk}(\mathbf{x}, \mathbf{y})$. From (20) the function f_1 enters in the Green tensor component through the following quantity

$$M_{jk}(\mathbf{x}, \mathbf{y}) = \mathcal{J}_{kl}\left[\delta_{3j} - x_3\frac{\partial}{\partial R'_j}\right]\frac{\partial\langle f_1\rangle}{\partial R'_l} \tag{96}$$

which can be expanded, for $\mathbf{x}$ and $\mathbf{y}$ on the distant particle surface, as

$$M_{jk}(\mathbf{x}, \mathbf{y}) \sim M_{jk}(\mathbf{x}_c, \mathbf{x}_c) + \left[\frac{\partial M_{jk}}{\partial R'_\alpha}(\mathbf{x}_c, \mathbf{x}_c)\right](x'_\alpha - y'_\alpha) + \left[\frac{\partial M_{jk}}{\partial x_3}(\mathbf{x}_c, \mathbf{x}_c)\right]x'_3 + \left[\frac{\partial M_{jk}}{\partial y_3}(\mathbf{x}_c, \mathbf{x}_c)\right]y'_3 \tag{97}$$

with a summation over indices $\alpha = 1, 2$ in (97). From the definition (94), one has

$$f_1 = f_1(\xi, y_3) = y_3 f_{1a}(\xi) + f_{1b}(\xi), \ f_{1a} = \frac{2\Lambda(\eta\xi - 1)}{1-S}, \ f_{1b} = -\frac{4\Lambda\eta}{1-S}. \tag{98}$$

Because $\mathbf{x}_c = d\mathbf{e}_3$, it immediately follows from (28)–(29) that

$$M_{jk}(\mathbf{x}, \mathbf{y}) = -\mathcal{J}_{kl}\left\{\delta_{j3}\delta_{l3}\int_0^\infty \xi e^{-2d\xi} f_1(\xi, d)\mathrm{d}\xi + dc_{jl}\int_0^\infty \xi^2 e^{-2d\xi} f_1(\xi, d)\mathrm{d}\xi\right\}, \tag{99}$$

$$\left[\frac{\partial M_{jk}}{\partial R'_\alpha}(\mathbf{x}_c, \mathbf{x}_c)\right] = \mathcal{J}_{kl}\left\{\delta_{j3}c_{\alpha l}\int_0^\infty \xi^2 e^{-2d\xi} f_1(\xi, d)\,\mathrm{d}\xi - d\,d_{\alpha jl}\int_0^\infty \xi^3 e^{-2d\xi} f_1(\xi, d)\,\mathrm{d}\xi\right\}. \tag{100}$$

In a similar way, exploiting the definition (96) and the decomposition (98) gives

$$\begin{aligned}\left[\frac{\partial M_{jk}}{\partial y_3}(\mathbf{x}_c, \mathbf{x}_c)\right] &= \delta_{j3}\mathcal{J}_{kl}[c_{3l}\int_0^\infty \xi^2 e^{-2d\xi} f_1(\xi, d)\,\mathrm{d}\xi - \delta_{l3}\int_0^\infty \xi e^{-2d\xi} f_{1a}(\xi)\,\mathrm{d}\xi] \\ &\quad -d\,\mathcal{J}_{kl}[c_{lj}\int_0^\infty \xi^2 e^{-2d\xi} f_{1a}(\xi)\,\mathrm{d}\xi + d_{3jl}\int_0^\infty \xi^3 e^{-2d\xi} f_1(\xi, d)\,\mathrm{d}\xi],\end{aligned} \tag{101}$$

$$\begin{aligned}\left[\frac{\partial M_{jk}}{\partial x_3}(\mathbf{x}_c, \mathbf{x}_c)\right] &= \delta_{j3}\mathcal{J}_{kl}c_{3l}\int_0^\infty \xi^2 e^{-2d\xi} f_1(\xi, d)\,\mathrm{d}\xi \\ &\quad -\mathcal{J}_{kl}\left[c_{lj}\int_0^\infty \xi^2 e^{-2d\xi} f_1(\xi, d)\,\mathrm{d}\xi + d\,d_{3jl}\int_0^\infty \xi^3 e^{-2d\xi} f_1(\xi, d)\,\mathrm{d}\xi\right].\end{aligned} \tag{102}$$

The integrals in the right-hand sides of (99)–(102) are approximated for large $\lambda = 2d$ by appealing to the formula (34). Using here the expansions

$$\int_0^\infty e^{-2d\xi}\xi f(\xi)\mathrm{d}\xi = \frac{f(0)}{4d^2} + \frac{f'(0)}{4d^3} + \mathrm{o}\left(\frac{1}{d^3}\right), \tag{103}$$

$$\int_0^\infty e^{-2d\xi}\xi^2 f(\xi)\mathrm{d}\xi = \frac{f(0)}{4d^3} + \frac{3f'(0)}{8d^4} + o\left(\frac{1}{d^4}\right), \tag{104}$$

$$\int_0^\infty e^{-2d\xi}\xi^3 f(\xi)\mathrm{d}\xi = \frac{3f(0)}{8d^4} + o\left(\frac{1}{d^4}\right) \tag{105}$$

and identities

$$f_{1a}(0) = -2,\ f'_{1a}(0) = \frac{4\sqrt{K}}{\sigma}\left(1 + \frac{\sigma\sqrt{K}}{e}\right),\ f_{1b}(0) = -\frac{4\sqrt{K}}{\sigma} \tag{106}$$

one then obtains

$$\begin{aligned} M_{jk}(\mathbf{x},\mathbf{y}) \sim\ & \frac{1}{2d}\mathcal{J}_{kl}[\delta_{3j}\delta_{3l} + c_{jl}] \\ & -\frac{1}{d^2}\mathcal{J}_{kl}\frac{\sqrt{K}}{\sigma}\left[\delta_{3j}\delta_{3l}\frac{\sigma\sqrt{K}}{e} + \frac{c_{jl}}{2}\left(1 + 3\frac{\sigma\sqrt{K}}{e}\right)\right] \\ & +\frac{1}{4d^2}\mathcal{J}_{kl}[-2\delta_{3j}c_{\alpha l} + 3d_{\alpha jl}](x'_\alpha - y'_\alpha) \\ & +\frac{1}{2d^2}\mathcal{J}_{kl}\left[-\delta_{3j}c_{3l} + \frac{3}{2}d_{3jl} + c_{jl}\right](x'_3 + y'_3) + \frac{1}{2d^2}\mathcal{J}_{k3}\delta_{3j}y'_3. \end{aligned} \tag{107}$$

Appendix C

This Appendix shows that adding to a solution $\mathbf{d}_0$ a constant multiple of the unit normal $\mathbf{n}$ does not affect the vector $\int_S(\mathbf{W}\cdot\mathbf{y}')\cdot\mathbf{d}_0(\mathbf{y}')\mathrm{d}S$ whatever be the particle shape. This is done by proving the identity

$$\mathbf{V} = \int_S (\mathbf{W}\cdot\mathbf{y}')\cdot\mathbf{n}(\mathbf{y}')\mathrm{d}S = \mathbf{0}. \tag{108}$$

Setting $V_i = \mathbf{V}\cdot\mathbf{e}_i, n_j = \mathbf{n}\cdot\mathbf{e}_j$ and $y'_k = \mathbf{y}'\cdot\mathbf{e}_k$, we immediately obtain

$$V_i = \int_S W_{ijk}y'_k n_j \mathrm{d}S = \int_{\mathcal{P}} \boldsymbol{\nabla}\cdot\mathbf{v}^{(i)}\mathrm{d}\Omega \tag{109}$$

with $\mathbf{v}^{(i)}\cdot\mathbf{e}_j = W_{ijk}y'_k$. Hence, $\boldsymbol{\nabla}\cdot\mathbf{v}^{(i)} = W_{i11} + W_{i22} + W_{i33}$. From the definitions (38)–(39), this shows that $\boldsymbol{\nabla}\cdot\mathbf{v}^{(i)} = 0$, i.e. (108) holds.

References

1. Khabthani, S., Sellier, A., Elsami, L., Feuillebois, F.: Motion of a solid particle in a shear flow along a porous slab. J. Fluid Mech. **713**, 271–306 (2012)
2. Navier, C.L.M.H.: Mémoire sur les lois du mouvement des fluides. Mémoire de l'Académie Royale Des Sciences de l'Institut de France **6**, 389–440 (1823)

3. Churaev, N.V., Sobolev, V.D., Somov, A.N.: Slippage of liquids over lyophobic solid surfaces. J. Colloid Int. Sci. **97**, 574–581 (1994)
4. Baudry, J., Charlaix, E., Tonck, A., Mazuyer, D.: Experimental evidence for a large slip effect at a nonwetting fluid–solid interface. Langmuir **17**, 5232–5236 (2001)
5. Beavers, G., Joseph, D.: Boundary conditions at a naturally permeable wall. J. Fluid Mech. **30**, 197–207 (1967)
6. Saffman, P.G.: On the boundary condition at the surface of a porous medium. Stud. Appl. Math. **50**, 50–93 (1971)
7. Goren, S.L.: The hydrodynamic force resisting the approach of a sphere to a plane permeable wall. J. Colloid Interface Sci. **69**(1), 78–85 (1979)
8. Nir, A.: On the departure of a sphere from contact with a permeable membrane. J. Eng. Math. **15**(1), 65–75 (1981)
9. Sherwood, J.D.: The force on a sphere pulled away from a permeable half-space. Physico-Chem. Hydrodyn. **10**, 3–12 (1988)
10. Feuillebois, F., Loussaief, H., Pasol, L.: Particles in creeping flow near a slip wall. In: Todorov, M.D., Christov, C.I. (eds.) CP1186, Applications of Mathematics in Technical and Natural Sciences, pp. 3–14. American Institute of Physics, USA (2009)
11. Feuillebois, F., Ghalia, N., Sellier, A., Elasmi, L.: Motion of particles in a parabolic flow near a slip wall. In: Todorov, M.D., Christov, C.I. (eds.) CP1404, Applications of Mathematics in Technical and Natural Sciences, pp. 340–351. American Institute of Physics, USA (2011)
12. Chaoui, M., Feuillebois, F.: Creeping flow around a sphere in a shear flow close to a wall. Q. J. Mech. Appl. Math. **56**(3), 381–410 (2003)
13. Feuillebois, F., Loussaief, H.: Analytical solution for a spherical particle in a linear shear flow close a slipping wall. *To be submitted*
14. Sellier, A.: Asymptotic expansion of a class of integrals. Proc. R. Soc. Lond. A **445**, 69–98 (1994)
15. Blake, J.R.: A note on the image system for a Stokeslet in a no-slip boundary. Proc. Camb. Phil. Soc. **70**, 303–310 (1971)
16. Pozrikidis, C.: Boundary integral and singularity methods for linearized viscous flow. Cambridge University Press, Cambridge (1992)
17. Happel, J., Brenner, H.: Low Reynolds Number Hydrodynamics. Boston, Dordrecht (1991)
18. Faxen, H.: Der Widerstand gegen die Bewegung einer starren Kugel in einer zahen Flussigkeit, die zwischen zwei parallelen, ebenen Wanden eingeschlossen ist. Arkiv Mat. Astron. Fys. **18**(29), 1–52 (1924)
19. Pasol, L., Sellier, A., Feuillebois, F.: A sphere in a second degree polynomial creeping flow parallel to a wall. Q. J. Mech. Appl. Maths **59**, 587–614 (2006)

S. Khabthani
Laboratoire Ingénierie Mathématique
École Polytechnique de Tunisie
rue El Khawarezmi
743 La Marsa
Tunisia

A. Sellier
LadHyX
École Polytechnique
91128 Palaiseau Cedex
France
e-mail: sellier@ladhyx.polytechnique.fr

F. Feuillebois
LIMSI-CNRS
UPR 3251 B.P. 133
91403 Orsay Cedex
France

(Received: December 20, 2012; revised: July 1, 2013)